



## 17 Abstract

18 Offshore Freshened Groundwater (OFG) reservoirs are gaining attention, as evidence suggests  
19 they are more prevalent worldwide than previously thought. OFG systems are generally  
20 classified as either *passive*, a relic of ancient, lower sea levels, or as *active*, with an onshore-  
21 offshore hydrogeologic connection and associated discharge offshore. Previous studies on the  
22 mechanisms of OFG were conducted in various hydrogeologic settings, but the role of faults  
23 remains understudied. Based on geologic data, we apply hydrogeologic modeling of a faulted  
24 submarine confined aquifer in the Levant basin (eastern Mediterranean), to study the impact of  
25 faults on OFG. We find that faults that are close to the coastline and within the brackish zone  
26 that would have developed without a fault control the offshore salinities regardless of initial  
27 conditions. The influence of distal faults, in contrast, depends on antecedent conditions. When  
28 initial salinities are such that the distal fault lies in the fresh part of the aquifer, the saline wedge  
29 migrates landward toward the fault with sea-level rise, and the fault dictates the steady-state  
30 salinity distribution. If the fault is initially within the saline part of the aquifer, freshwater never  
31 reaches the fault, likely due to the density-driven flow barrier that the underlying saline wedge  
32 generates. These findings suggest a new mode of OFG in which the same geologic system can be  
33 either active or passive depending on the hydrologic history. This should be considered in future  
34 studies of OFG systems, the functioning of which has implications for marine ecosystems,  
35 seafloor geomorphology, and coastal water resources.

36

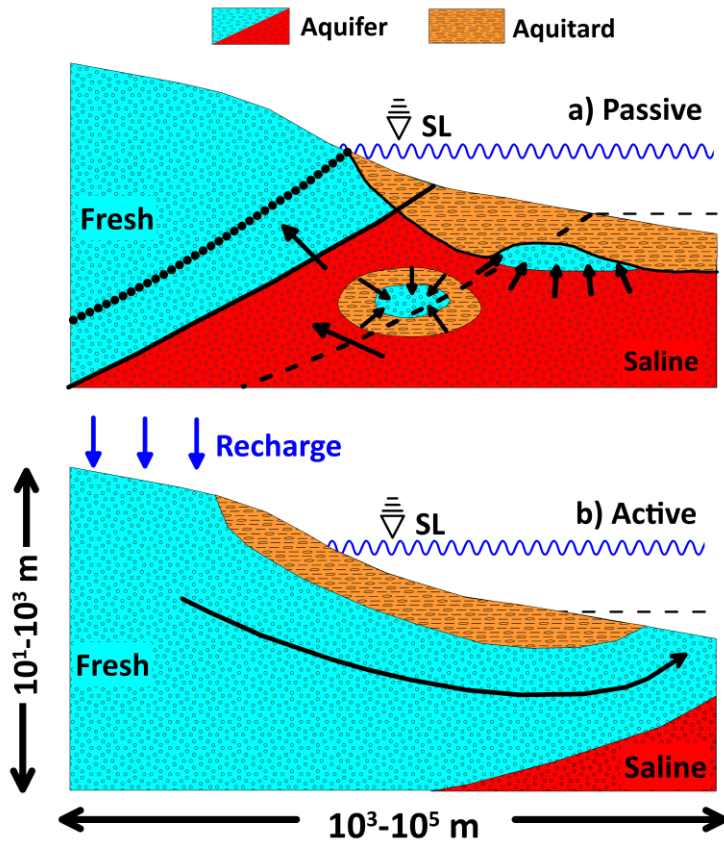
## 37 1. Introduction

38 Over the past decades, Offshore Freshened Groundwater (OFG) has been increasingly  
39 observed around the world (Post et al. 2013) in distal (>1 km offshore) and deep (>100 m water  
40 depth) submarine environments, including Hawaii (Attias et al., 2021), Malta (Haroon et al.,  
41 2021), New-Zealand (Micallef et al., 2020), and Israel (Paldor, et al., 2020a). The existence of  
42 these reservoirs is difficult to explain, since contemporaneous hydraulic heads on land are  
43 generally assumed to be too low to push terrestrial groundwater far offshore (Kooi & Groen,  
44 2001; Person et al., 2003; Post et al., 2013). Until recently, this assumption led researchers to  
45 believe that OFG reservoirs are not in steady state with the current hydrological state, but are  
46 relics of ancient systems with lower sea levels and/or elevated glacial heads on land, after which  
47 fresh groundwater was trapped when sea level rose to its modern location (Post et al., 2013).  
48 Such systems are classified as *passive* OFG, because there is no direct flow from the terrestrial  
49 recharge area to an offshore discharge area with an associated OFG reservoir (Fig. 1a). In recent  
50 years, mounting evidence suggests that *active* OFG reservoirs are also plausible under certain  
51 hydrogeological conditions, with direct onshore-offshore flow in deeper, subsea aquifers (Fig.  
52 1b). Such conditions have been observed in several geological settings around the world. Ancient  
53 lava tubes provide the onshore-offshore connectivity to transport terrestrial fresh groundwater  
54 offshore in a volcanic aquifer in Hawaii (Attias et al., 2021, 2020; Geng and Michael, 2020).  
55 Offshore the U.S. Atlantic margin, a subsea aquifer is connected to the ocean through a  
56 monoclinical structure, facilitating a direct land-to-sea flowpath that brings freshened groundwater  
57 to distal areas offshore (Gustafson et al., 2019). In New Zealand, freshened groundwater has  
58 been recently observed tens of kilometers offshore, and attributed to meteoric recharge into a  
59 fluvial aquifer that extends offshore. In the easternmost part of the Mediterranean Sea (hereafter  
60 referred to as the Levant basin), a confined carbonate aquifer exposed on the seabed along a  
61 submarine canyon was shown to produce discharge of freshened groundwater ~5 km offshore

62 (Paldor et al., 2020a; Paldor et al., 2019). These seeps are spatially associated with submarine  
 63 canyons, which align with previous observations of active OFG inducing submarine landslides  
 64 (Kelner et al., 2016; Oehler et al., 2017; Sultan et al., 2020).

65 A fundamental difference between active and passive OFG systems as a resource is related to  
 66 their renewability. Passive OFG reservoirs are finite and likely shrinking with time, due to  
 67 diffusive escape of the trapped freshened groundwater, and slow landward movement of the  
 68 freshwater-saltwater interface, as the system moves toward steady state with present-day sea  
 69 level. Conversely, active OFG reservoirs are constantly replenished from the land under modern  
 70 hydrologic conditions, and are likely more viable for extraction in the long term. The recent  
 71 discoveries of active OFG systems (Figure 1b) mentioned above merit further exploration, and a  
 72 deeper understanding of the underlying physics is necessary to better assess the viability of  
 73 active OFG as a freshwater resource and its ecological and geomorphological influence. The  
 74 above-mentioned two types of systems (active and passive, Fig. 1), have been considered  
 75 separately as the only plausible mechanisms for OFG, though they could occur together in  
 76 different parts of the same system. The assumption is that the geologic and hydrologic conditions  
 77 together control the functioning, whether passive or active. The possibility that the same  
 78 hydrogeologic system can be either active or passive depending on its antecedent hydrologic  
 79 conditions has not been considered previously.

80



81  
 82 *Figure 1: A conceptual illustration of (a) passive and (b) active systems of OFG. In panel (a)*  
 83 *arrows mark the shrinking/recession of fresh groundwater. In panel (b), the*  
 84 *arrow is the regional-scale trajectory of fresh groundwater from terrestrial recharge to offshore discharge.*

85 Beyond their value for human consumption, active OFG reservoirs have the potential to impact  
86 ecosystem functioning as fresh groundwater discharge affects chemical budgets and nutrient  
87 supply in the ocean (Li et al., 1999; Luijendijk et al., 2020; Moore, 2010). In the Levant basin,  
88 the discharge point of the recently discovered active OFG system (Paldor et al., 2020a) coincides  
89 with an area of high biologic activity (Elasar et al., 2013). In addition to the biogeochemical  
90 importance of submarine groundwater discharge, the seepage force that is exerted by the  
91 discharging groundwater has the potential to destabilize the seafloor and control its morphology  
92 (Micallef et al., 2023; Iverson & Reid, 1992; Oehler et al., 2017; Schorghofer et al., 2004;  
93 Stegmann et al., 2011). The Levantine system occurs in an area that is characterized by unique  
94 seafloor morphology of regularly spaced submarine canyons. A causal relationship between  
95 submarine groundwater discharge and submarine canyon formation has been suggested in  
96 several places around the world (Cohen et al., 2010; Dugan & Flemings, 2002; Orange et al.,  
97 1994, 2002; Paldor, et al., 2020b), and has recently been quantified on a global scale (Micallef et  
98 al., 2023). Since active OFG systems likely feature active discharge (Figure 1b), understanding  
99 their underlying dynamics is important to assess the implications for ecosystem functioning and  
100 seafloor geomorphology, not only for their potential as a freshwater resource. Lastly, an  
101 important angle in the discussion on the value of OFG is their potential to serve in oil production.  
102 It has been suggested that freshwater can be injected into offshore oil reservoirs to improve oil  
103 recovery, and that OFG may be used for this process to reduce costs of transporting fluids from  
104 onshore (Person et al., 2017). However, this bears collateral environmental implications both  
105 onshore and offshore (Yu & Michael, 2019). To better assess these implications, the underlying  
106 physics of OFG systems must be rigorously investigated.

107 In many countries along the Mediterranean coastline, and in the Levant basin particularly,  
108 karstic aquifers are one of the important sources of freshwater. In Lebanon, the Cretaceous  
109 karstic aquifer has been shown to produce submarine groundwater discharge close to the  
110 coastline (<1 km) and is considered a major component in the terrestrial water balance,  
111 potentially transporting vast amounts of fresh groundwater to the sea (Bakalowicz et al., 2008;  
112 Fleury et al., 2007; Shaban et al., 2005). In northern Israel, the Cretaceous aquifer is exposed on  
113 land and receives substantial portions of the recharge in that area. This aquifer is known to  
114 discharge groundwater on land along springs, but until recently, some of the recharge was  
115 unaccounted for and researchers were unable to close the water balance (Kafri & Kessler, 2001).  
116 A recent study showed that the aquifer outcrops far offshore (~5 km) along a submarine canyon,  
117 and that this subsurface hydraulic connection causes losses of terrestrial water to the  
118 Mediterranean sea (Paldor et al., 2020a; Paldor et al., 2019). These findings emphasize that in the  
119 Levant region and in the Mediterranean more generally, understanding of the onshore-offshore  
120 hydrogeological conditions is vital for water resources management, especially with the arid  
121 climate that characterizes much of this region.

122 While active OFG systems have been found in several geological settings around the world,  
123 previous studies do not consider the potential role of submarine faults. On nearshore scales (on  
124 the order of tens of meters from the coastline), which correspond to shallow, phreatic aquifers  
125 (Bratton, 2010), faults have been shown to impact the dynamics of saltwater intrusion and  
126 submarine groundwater discharge. For example, modeling an idealized geometry revealed that  
127 flow rates and salinities in a submarine spring are strongly sensitive to the characteristics of a  
128 discrete flow conduit within the hypothetical aquifer (Xu et al., 2018). Similarly, a generalized  
129 model of a fractured coastal aquifer demonstrated the strong control of the fracture-network  
130 configuration on the rates of pumping-induced saltwater intrusion (Sebben et al., 2015). The

131 effect of fractures has also been observed in natural conditions. In the Levant, remote sensing  
132 revealed thermal anomalies that suggested a spatial relationship between faults and nearshore  
133 submarine groundwater discharge (Shaban et al., 2005). Despite these important contributions,  
134 hydrogeological modeling of submarine faults in a real system is still needed to better understand  
135 their potential role in facilitating OFG.

136 This work aims to address two critical open research questions: 1) what is the hydrogeological  
137 functioning of faults in OFG systems, and 2) can a given geological setting form an OFG system  
138 that is either active or passive, depending on antecedent hydrologic conditions? To address these  
139 questions, we conducted a detailed geological interpretation of an onshore-offshore system in the  
140 Levant basin, including mapping of offshore faults. Based on the interpreted geological data and  
141 the structural setting of the mapped aquifers, 2D hydrogeological modeling was applied to  
142 analyze the processes that dominate the dynamics of OFG in that system, and the role of faults.  
143 Calibrated model parameters were taken from previous studies in the region (Dafny et al., 2010;  
144 Kafri, 1970; Paldor et al., 2020a; Paldor et al., 2020b; Paldor et al., 2019). To generalize our  
145 findings, we also simulated various scenarios of faulting and antecedent conditions to explore the  
146 global applicability of our models and the mechanisms they demonstrate. The results presented  
147 here therefore provide insights for the exploration of OFG reservoirs worldwide, with important  
148 global implications for water resources management, seafloor geomorphology, and marine  
149 biogeochemistry.

150

## 151 **2. (Hydro)Geological setting**

152 The Levant Basin is located in the eastern Mediterranean Sea (Figure 2A) at the intersection of  
153 three plates, i.e. the Arabian, African and Eurasian Plate (Vidal et al., 2000; Stacey, 2021). The  
154 Basin formed in the Early Mesozoic, as regional geologic rifting occurred in the entire Tethys  
155 area (Dewey et al., 1973; Garfunkel and Derin, 1984). At this time, the basin was characterized  
156 by shallow platform carbonates in the east and by deep-water carbonates on the slope and basin  
157 in the west (Bein and Gvirtzman, 1977; Druckman et al., 1995, Garfunkel, 1998). The Late-  
158 Jurassic to Mid-Cretaceous shallow platform carbonates host the main aquifers of the Levant  
159 region. These formations transition, westwards of a ‘hinge line’, to deep marine setting and fine-  
160 grained, impermeable lithologies called “Talme Yafe” (Gardosh et al., 2008) (Figure 2C).

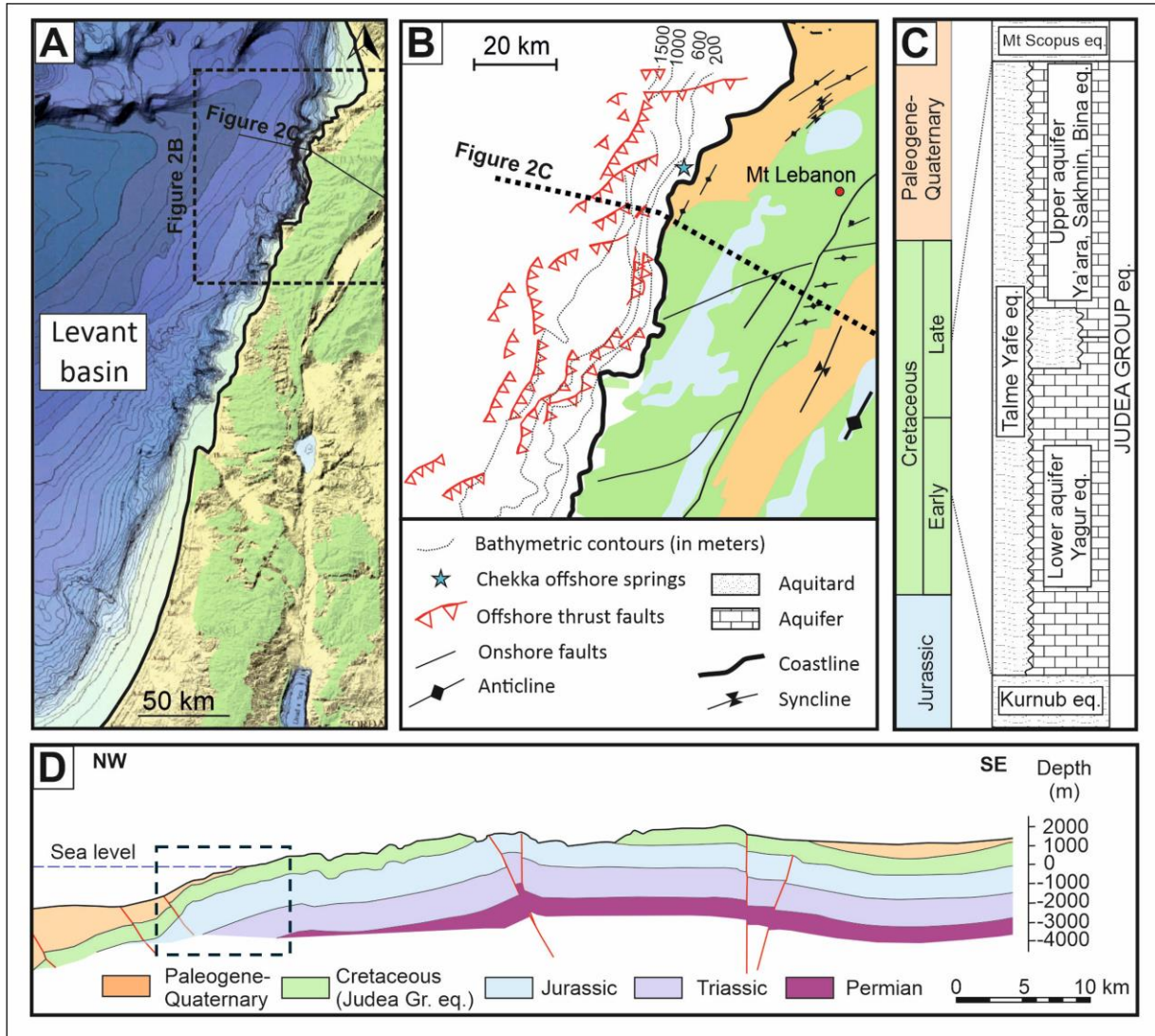
161 The Mesozoic karst aquifer that is the focus of this study is composed of numerous lithologies  
162 (Fig. 2), with the Judea Group (Gardosh and Druckman, 2006) being its uppermost  
163 hydrostratigraphic unit (green polygons in Fig. 2A and B). Traditionally, the Judea Group is  
164 divided into two sub-aquifers. The lower sub-aquifer is formed by the ‘Yagur’ Formation, and  
165 the upper sub-aquifer comprises the ‘Ya’ara’ Member (Dier Hanna Formation), Sakhnin  
166 Formation and Bina Formation (Kafri, 1972, Kafri and Fleischer, 2003; Dafny et al., 2010).  
167 These sub-aquifers are separated by a leaky aquitard of the Moza and Bet-Me’ir Formations  
168 (Dafny et al., 2010). As the aquitard is discontinuous, the Judea Group is often considered one  
169 single aquifer of thickness ~600m bounded from below by the Kurnub Group aquitard (Gardosh  
170 et al., 2008). This work assumes this simplification and a uniform aquifer is considered hereafter.  
171 The Judea Group transitions into the aforementioned impermeable Talme Yafe Formation, with  
172 this lateral boundary located further offshore of our modelling area, therefore not included in the  
173 model.

174 Today, the Judea Group aquifer is overlain by the Mt. Scopus Group of Senonian age, and the  
175 Saqiye Group that was deposited throughout the Tertiary. The lithologies of both these Post-  
176 Judea rock units are considered nearly-impervious, with hydraulic conductivities about 3 orders

177 of magnitude lower than the Judea Group aquifer (Dafny et al., 2010; Kafri & Fleischer, 2003;  
178 Kafri, 1972). The Judea Group outcrops on land (green polygons in Fig. 2) along the Lebanese  
179 coastal plain and Mount Lebanon that rises up to a height of ~1500 m. Annual rainfall is  
180 currently around 800 mm, providing the primary source of recharge into the aquifer. Past climate  
181 conditions likely included different rainfall rates, but with the lack of other information, the  
182 present value was adopted in the model described below. During the late Tertiary, several  
183 tectonic phases and relative sea-level changes controlled the post-depositional evolution of the  
184 Mesozoic aquifer, which has experienced tectonic deformation and karstification, forming an  
185 extensive conduit system through which fresh/brackish water flows (Ghannam et al., 1998;  
186 Shaban et al., 2005). We mapped submarine faults that cut through the Judea group (red lines in  
187 Figure 2 a&b), based on seismic data analyzed in previous studies (Carton, 2009; Hawie et al.,  
188 2013). The structure presented here has been verified in previous studies from the region  
189 (Carton, 2009; Haiwe et al., 2013), including the offshore faults, and the velocities used for time  
190 to depth conversion of the seismic reflection profiles have similarly been previously established  
191 (Druckman, 2006). We therefore adopt the interpreted structure (Fig. 2D) and apply a  
192 groundwater model according to it, as detailed in section 3 below. The naming of the geological  
193 units adopted here follows the notion of the Geological Survey of Israel, whereas in Lebanon the  
194 Cretaceous limestone, chalk and marl units which are time-equivalent of the Judea group are  
195 named Mdairej (Lower Cretaceous), Hammama, Sannine and Maameltain and part of the Chekka  
196 Fm. (Upper Cretaceous)

197 A shallow coastal aquifer also exists in the area, hosted by the Quaternary Kurkar formation.  
198 Compared to the Mesozoic carbonate aquifer, this aquifer has limited recharge area and total  
199 storage capacity, and large lithological heterogeneity with related differences in hydraulic  
200 conductivities (Vengosh & Ben-Zvi 1994; Avisar et al., 2004). Furthermore, the offshore extent  
201 of this aquifer is limited to the typical nearshore extents of shallow aquifers, on the order of 1-10  
202 m from the coastline (Bratton, 2010). Hence, in the context of deep OFG systems, this local

203 system is neglected from the current study, and the entire post-Judea column is considered  
 204 uniformly as an aquitard (Paleogene-Quaternary in Fig. 2).  
 205



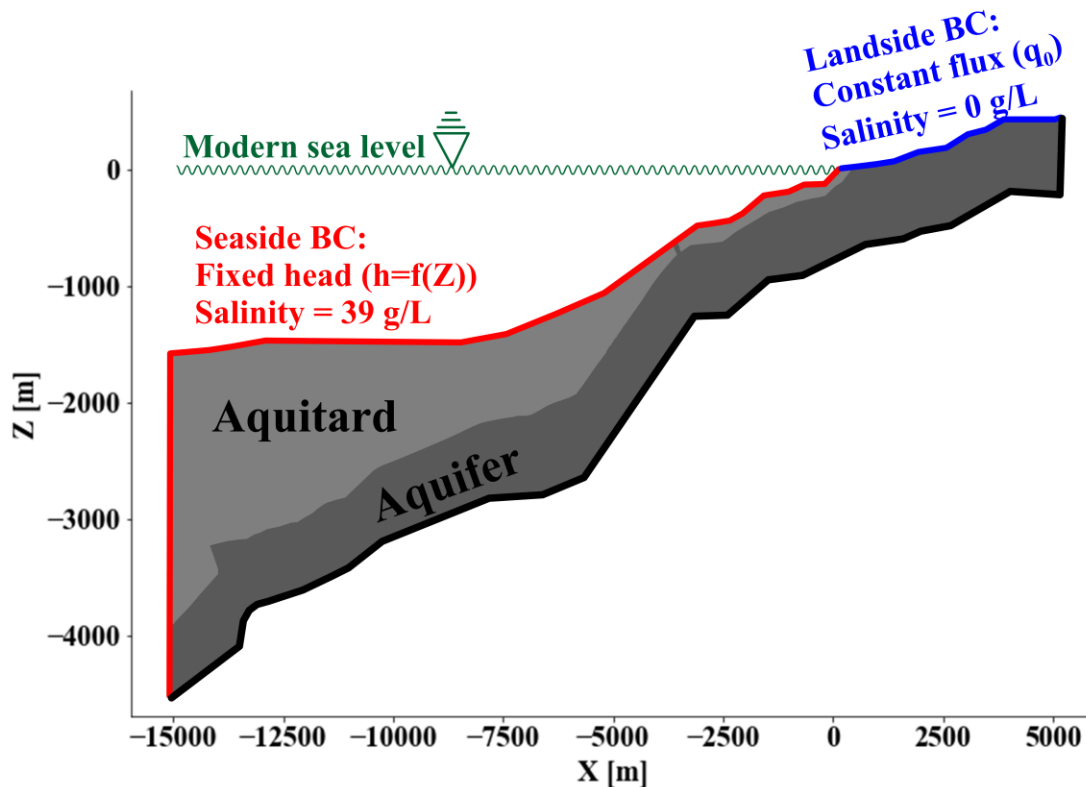
206  
 207 *Figure 2: (A) Regional map and bathymetry of the Levant basin. (B) General fault regimes in*  
 208 *Lebanon. The onshore strike-slip faults, roughly trending E-W, are in thin black, as well as the*  
 209 *major elements of the Dead Sea Fault System (Walley, 2004). Tertiary thrusts have been found up*  
 210 *to 30km offshore (Carton et al., 2009) and are shown in red. These faults trend NE-SW and bend*  
 211 *around in northern Lebanon as part of the restraining bend. (C) A columnar lithologic section*  
 212 *detailing the geological units interpreted here (note that nomenclature follows the Geological*  
 213 *Survey of Israel). (D) The geological cross-section that is the focus of the current study, compiled*  
 214 *based on Ghalayini et al. (2017, 2018 (Petroleum systems of Lebanon)) for the onshore cross-*  
 215 *section and Hawie et al. (2013), Carton et al. (2009) for the offshore part of the section, see text*  
 216 *for an explanation on time-depth conversion. The domain taken for the FEFLOW model is marked*  
 217 *with a black dashed frame, including the observed offshore fault in red. A blue dashed line marks*  
 218 *the sea level (SL).*

219 **3. FEFLOW model**

220 Based on the inferred geological structure (Fig. 2D) we designed a hydrogeological model  
 221 using FEFLOW (Fig. 3), a finite-element numerical code that simulates groundwater flow and  
 222 salt transport. FEFLOW accounts for variable-density flow by coupling simulated salinities with  
 223 heads through a linear equation of state. The maximum salinity in the model was taken as the  
 224 Mediterranean Sea average salinity (39 g/L), with a corresponding maximum density of 1029  
 225 kg/m<sup>3</sup>. These values are based on previous measurements of seawater in the same area (Paldor et  
 226 al., 2020a). For boundary conditions, the land surface (blue line in Fig. 3) was assigned a  
 227 constant freshwater flux, taken as 20% of the precipitation, consistent with previous estimates  
 228 from the region (Kessler & Kafri, 2008; Paldor et al., 2019; Yechieli et al., 2009). The seaside  
 229 boundary (red line in Fig. 3) was simulated with a constant seawater salinity and a fixed  
 230 freshwater-equivalent head that varied with depth as:

$$h(Z) = -\alpha \cdot Z$$

231 where the factor  $\alpha$ , called density ratio, accounts for the higher seawater density and is defined  
 232 as  $\alpha = \frac{\rho_s - \rho_f}{\rho_f} = 0.029$  (assuming freshwater density of  $\rho_f = 1000 \text{ kg/m}^3$ ). Applying a depth-  
 233 dependent freshwater head along the seafloor is a widely-adopted approach in coastal/marine  
 234 hydrogeology (e.g. Kooi and Groen, 2001; Person et al., 2003; Paldor et al., 2022; Stanic et al.,  
 235 2024). This assumes hydrostatic conditions along the seafloor, such that the saltwater head is  
 236 zero. Since the thickness of the (salt)water column varies with the depth of the seafloor, the  
 237 freshwater-equivalent head is greater than zero as the pressure head increases more rapidly than  
 238 the gravitational head due to the higher density of saltwater. The other model boundaries (black line in Fig. 3)  
 239 were assumed zero-flux for both fluid and salt.  
 240  
 241



242  
 243 *Figure 3: FEFLOW model setup and boundary conditions. The confined aquifer (shaded area)*  
 244 *and the overlying aquitard follow the interpreted structure (Fig. 2). The function that defines the*

245 head-depth relationship on the seafloor is  $f(Z) = -\alpha Z$ , where  $\alpha$  is the density ratio. See text for  
 246 details.

247  
 248 The aquifer and the overlying confining aquitard (Fig. 3) were assigned isotropic hydraulic  
 249 conductivities of 50 m/d and 0.01 m/d, respectively. These values are consistent with previous  
 250 models from the same area (Kafri & Kessler, 2001; Paldor et al., 2019). All other model  
 251 parameters are given in Table 1.

252  
 253 *Table 1: Model parameters.*

Parameter	Symbol	Unit	Value	Source
Aquifer Hydraulic Conductivity	$K_a$	m/d	50	Paldor et al. (2019)
Aquitard Hydraulic Conductivity	$K_c$	m/d	0.01	Kafri & Kessler (2001)
Anisotropy	$K_x/K_z$	-	1	
Specific Storage	$S_s$	1/m	$10^{-4}$	Paldor et al. (2019)
Freshwater recharge	$q_0$	m/d	$1e-3$	Yechieli et al. (2009)
Porosity	$\phi$	-	0.3	
Specific storage	$S_s$	1/m	$1e-4$	Freeze & Cherry (1979)
Seawater density	$\rho_s$	$kg/m^3$	1029	
Longitudinal Dispersivity	$\alpha_L$	m	50	Gelhar et al. (1992)
Lateral Dispersivity	$\alpha_T$	m	5	Gelhar et al. (1992)

254  
 255 Faults were simulated as simple elements with straight geometry cutting through the confining  
 256 layer down to the aquifer, having the hydraulic conductivity of the aquifer (Table 1). Rather than  
 257 simulating faults as discrete elements, we incorporated them continuously as part of the isotropic  
 258 porous medium, with a thickness of 50-100 m to represent the typical faulting damage zones.  
 259 This simplified representation of faults is conservative in the sense of their effect on OFG, since  
 260 we neglect the potential impact of anisotropic K enhancing along-fault flow. Due to the  
 261 dynamics of slip during faulting, it is often assumed that the flow rate along the fault is orders of  
 262 magnitude higher than across it (Bense et al., 2013). Such anisotropy means that the fault-related  
 263 hydraulic connection between the confined aquifer and the sea could be much stronger than

264 simulated, which would likely strengthen the control of faults on OFG. Therefore, modeling the  
265 relationship between faults and OFG assuming isotropic K in the fault is a conservative  
266 approach. Simplifying the K in the fault also allowed increased numerical stability and  
267 drastically decreased runtimes. To capture a range of faulting scenarios, we simulated separately  
268 four fault configurations. The first configuration was of the observed fault, intersecting with the  
269 seafloor at a water depth of ~1000 mbsl (meters below sea level), and a distance of 5.4 km  
270 offshore. A second fault was simulated closer to the coastline, intersecting the seafloor at a  
271 distance of 3.7 km and a water depth of 600 mbsl. The third fault was simulated closest to the  
272 coastline, intersecting with the seafloor 2 km offshore and at a water depth of 350 m. Based on  
273 their distance from the coastline, we name these faults *distal*, *intermediate*, and *proximal*. These  
274 three faults were inclined at 40 degrees from the horizon, typical of compressional faults as the  
275 ones observed in the studied area (Fig. 2). A fourth fault was simulated at the same depth as the  
276 distal one (intersecting the seafloor at 1000 mbsl and 5.4 km offshore), but oriented vertically so  
277 that its midpoint is further offshore than the distal one. This generalizes our results beyond the  
278 local tectonic regime in the Levant Basin. Based on Anderson's theory of faulting, vertical faults  
279 typically occur in compressional tectonic regimes as strike-slip faults (Anderson, 1905). Since  
280 the faults were assigned hydraulic properties similar to the aquifer, they are apparent in the  
281 model only along the aquitard, as once they cut into to the aquifer they are essentially the same  
282 material as their host rock.

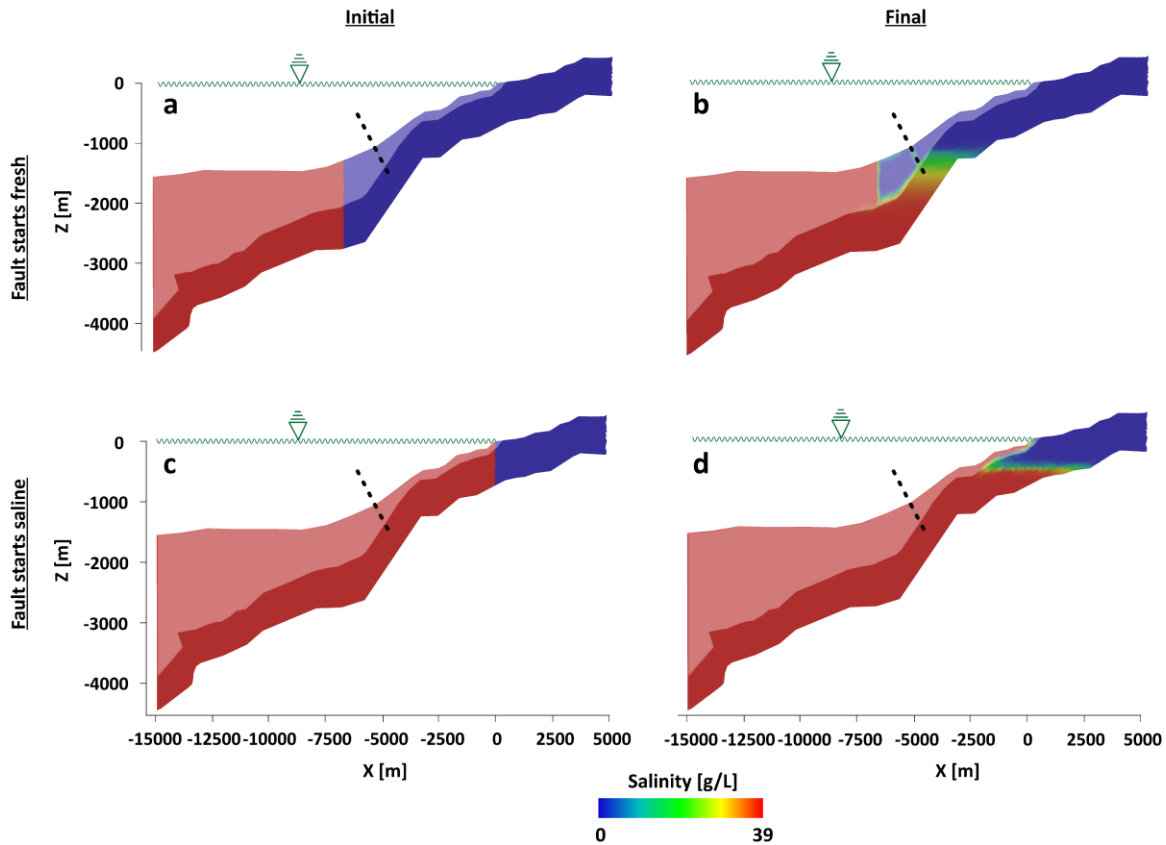
283 The model was run with two initial conditions for salinity: one in which the interface between  
284 fresh and saline groundwater was located seaward of the respective fault, such that the faults  
285 were initially within the fresh part of the aquifer (the interface was seaward of the fault), and  
286 another in which the fault location was initially saline (the interface was landward of the fault).  
287 In all simulations, the model was run to quasi-steady state, considered when heads and salinities  
288 in the aquifer were not changing with time. The salinities in the confining layer were not  
289 considered in our assessment of quasi-steady state, as the aquitard reaches steady state over time  
290 scales that are orders of magnitude higher than the aquifer, and beyond the scope of this work.

291

## 292 **4. Results**

### 293 4.1 The dependency of OFG on initial conditions

294 When the freshwater-saltwater interface is initially seaward of the distal fault, the steady-state  
295 salinity is such that freshened groundwater exists continuously from the recharge area on land to  
296 the fault (Fig. 4). If the initial conditions are such that the fault location is initially saline, then  
297 the fresh groundwater never reaches the fault (Fig. 4 c&d). Hence, this fault-dependent OFG is a  
298 combination of the two previously-considered types of OFG (Fig. 1). It features direct onshore-  
299 offshore geologic connectivity (namely, active OFG), but its existence in steady state with  
300 modern hydrological regimes requires antecedent conditions in which an OFG body extends to  
301 or past the fault. These fresh conditions are the same as required for passive systems, but in this  
302 case, they enable the existence of an active OFG. Without freshened antecedent conditions, the  
303 OFG does not exist, despite having geologic conditions conducive to active onshore-offshore  
304 freshwater flow. This suggests a novel mechanism for OFG that has not been previously  
305 considered, since all occurrences of OFG were categorized as either passive (Fig. 1a) or active  
306 (Fig. 1b). In other words, faults may generate onshore-offshore geologic connectivity, but  
307 onshore-offshore flow of freshened groundwater in steady state with modern hydrologic  
308 conditions requires initial emplacement in these fault-controlled systems. This important result  
309 and its potential implications are further discussed in Section 5 below.



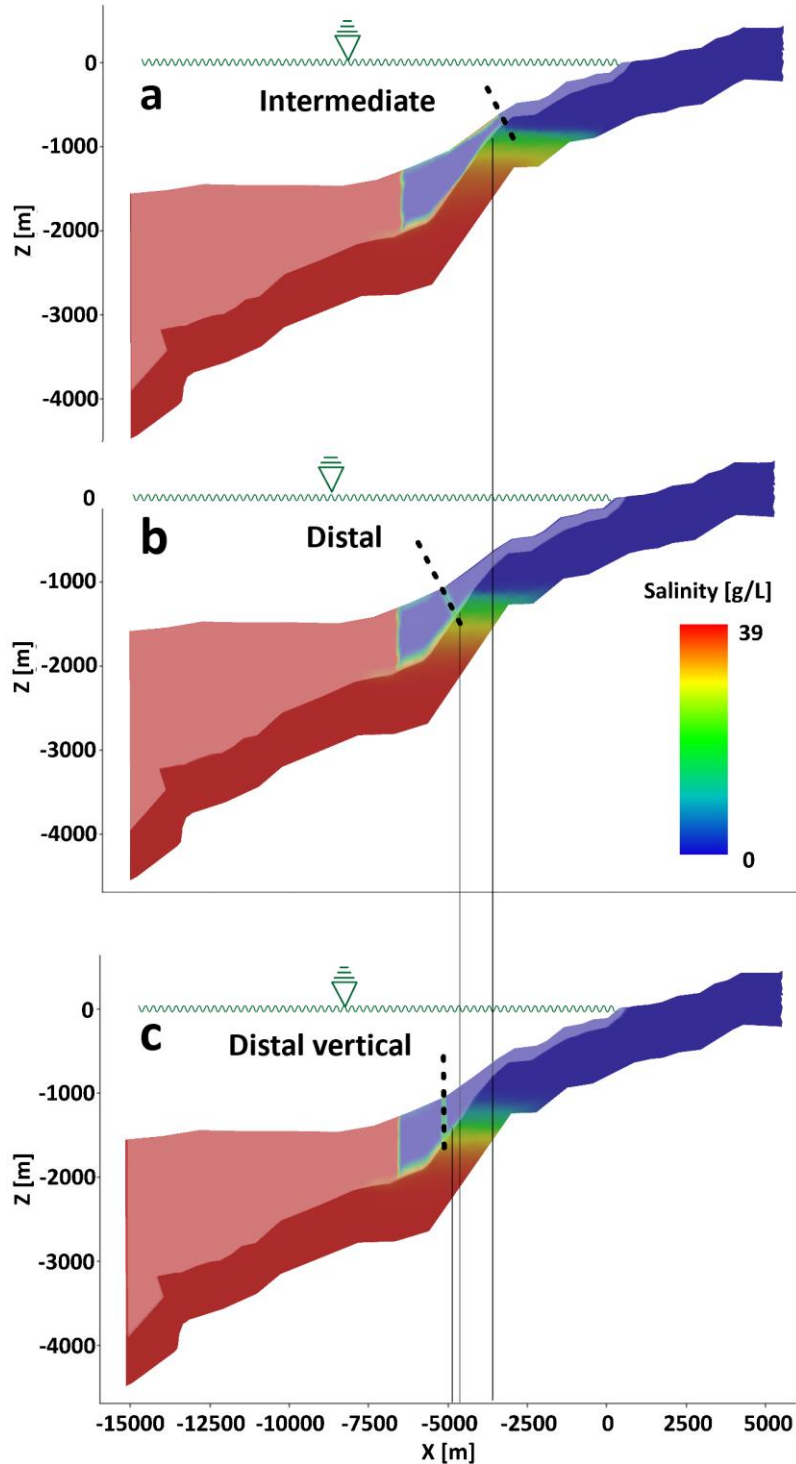
310  
 311 *Figure 4: Initial (left, panels a&c) and final (right, b&d) salinities with the furthest fault (distal)*  
 312 *starting fresh (top) and saline (bottom). The salinities in the aquitard are masked to distinguish*  
 313 *from the aquifer salinities. Note that the faults are marked here with a dashed line that extends*  
 314 *beyond the seafloor for visibility purposes only. See Section 3 above for detailed explanation of*  
 315 *the fault implementation in the model.*

#### 316 4.2 Fault location and geometry control OFG

317 For the case where the fault was initially fresh, the location of the fault along the shelf is found  
 318 to control the extent of OFG (Fig. 5). The intersection between the fault and the aquifer largely  
 319 controls the intersection between the 50% salinity contour and the top of the aquifer, such that  
 320 the distal fault brings the freshened groundwater ~650 m further into the basin compared to the  
 321 intermediate fault (Fig. 5 a&b). Since the intermediate fault is located ~1700 m closer to the  
 322 coastline than the distal fault, the difference in OFG extent (650 m) is much smaller than the  
 323 difference in fault location. It is also noted that there is a difference in the salinity distribution  
 324 around the fault between the two cases. In the case of the distal fault, the fresh-saline transition  
 325 zone evolved around the fault, meaning that the groundwater discharged through the fault is  
 326 brackish. In the intermediate fault, the transition zone is entirely seaward of the fault, meaning  
 327 that the fault cuts into the aquifer in an area where the salinities are much lower (compare Fig. 5a  
 328 with 5b - the intermediate fault intersects a blue region in the aquifer, whereas the distal fault  
 329 intersects a yellow region).

330 When the distal fault is simulated initially fresh but as a vertical fault (typical of strike-slip  
 331 faults in a compressional tectonic regime), there is a marginal effect on the OFG extent (Fig. 5  
 332 b&c). The OFG extent is controlled by the fault-aquifer intersection, such that with the vertical

333 fault, the maximum offshore distance of the 50% salinity contour in the aquifer is ~150 m greater  
334 than the inclined fault (black lines in Fig. 5b&c). While both faults intersect with the seafloor at  
335 the same point, the vertical fault intersects the top of the aquifer at X=-5400 m, and the inclined  
336 fault intersects at X=-4900 m. Thus, similar to the comparison between the distal and the  
337 intermediate faults, the difference in the OFG extent (~150 m) between the distal and the vertical  
338 faults is about 1/3 the difference in their fault-aquifer intersection locations (~500 m).



339  
 340  
 341  
 342  
 343  
 344  
 345  
 346

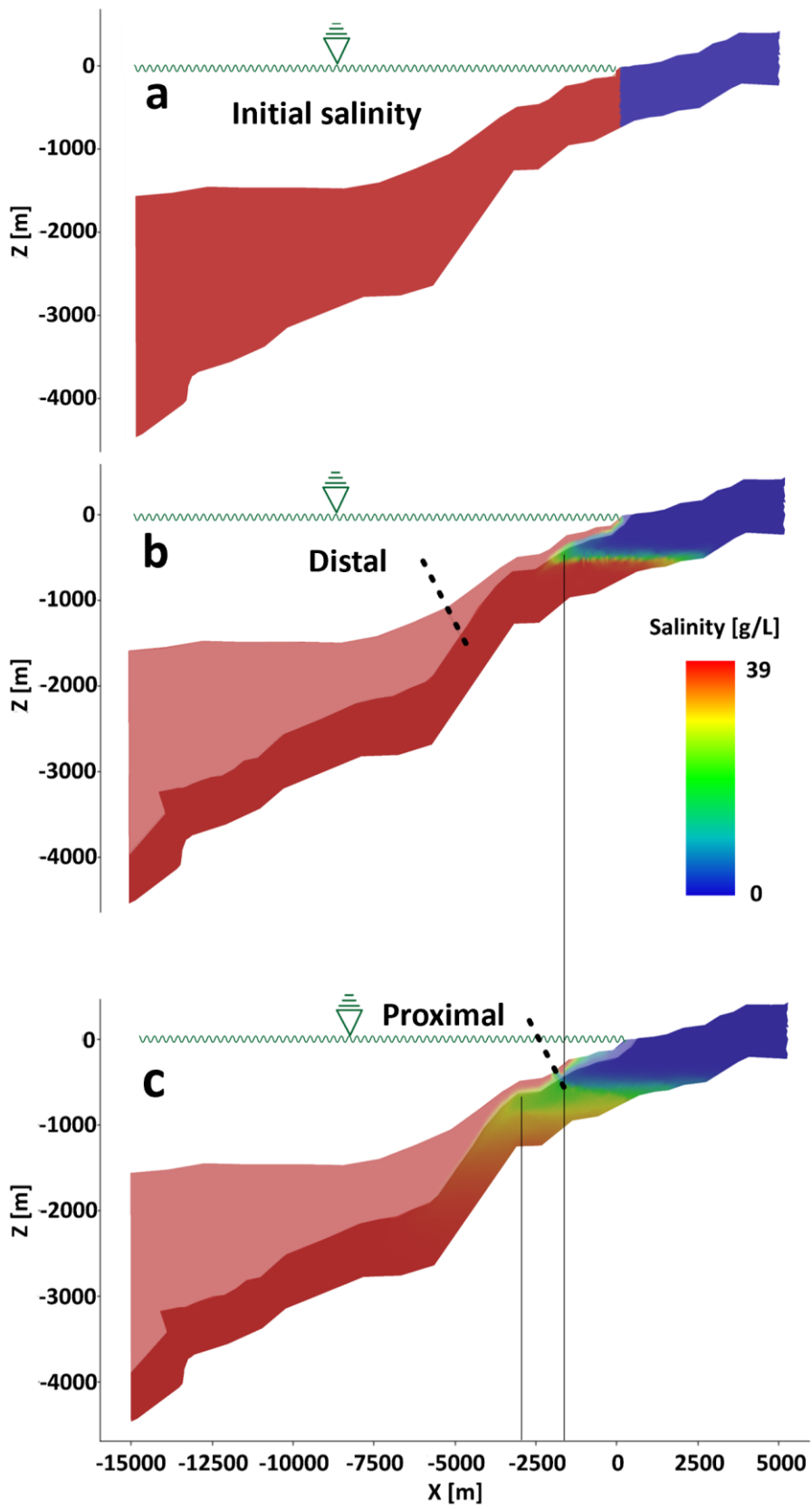
Figure 5: Final simulated salinities for three fault scenarios: (a) Intermediate distance offshore (fault intersects the seafloor at a water depth of 600 mbsl); (b) Distal (fault intersects the seafloor at 1000 mbsl) and (c) Distal vertical (fault intersects the seafloor at 1000 mbsl but its midpoint is further offshore). Vertical black lines denote the intersection of the 50% salinity contour and the top of the aquifer. In all cases plotted here, the initial interface is seaward of the fault (i.e., fault starts fresh). The salinities in the aquitard are masked to distinguish from the aquifer salinities. Note that the faults are marked here with a dashed line that extends beyond the

347 *seafloor for visibility purposes only. See Section 3 above for detailed explanation of the fault*  
348 *implementation in the model.*

349  
350 4.3 Proximal fault controls offshore salinity distribution regardless of initial conditions

351 When the fault is closest to the coastline (i.e., proximal fault), it controls the extent of OFG in  
352 steady state regardless of the initial salinity distribution (Fig. 6). This is in contrast to the distal  
353 fault, where an initially salty fault leads to final salinities that are independent of the fault, and  
354 the freshened groundwater never reaches it (Figure 6c). This means that there is a certain  
355 threshold for the offshore distance of the fault that dictates whether or not its relationship with  
356 the eventual OFG depends on initial salinities. This threshold distance depends on the transition  
357 zone that is simulated regardless of a fault (i.e., the transition zone that would have been  
358 simulated without any faults). When the proximal fault cuts the aquifer in an area that would  
359 have eventually been brackish regardless of faults, then the fault controls the final distribution of  
360 salt and the extent of OFG (Fig. 6b). This can be seen by the vertical line crossing from panels b  
361 and c in Fig. 6 – the steady-state brackish zone predicted regardless of faults (panel b) is at the  
362 same offshore distance as the intersection of the proximal fault with the aquifer (panel c). In both  
363 cases, the initial salinity was such that the entire aquifer was salty (panel a), but the final extent  
364 of OFG in the aquifer is ~2000 m with the distal fault, and ~3000 m with the proximal fault.  
365 Furthermore, when the fault is proximal enough to control the final salinity Fig. 6c), the  
366 transition zone is widened significantly compared to the transition zone that develops  
367 independent of faults (Fig. 6c). This is likely because the proximal fault acts as an outlet for  
368 freshened groundwater from the aquifer to the sea, allowing greater flow velocities and therefore  
369 higher hydrodynamic dispersion.

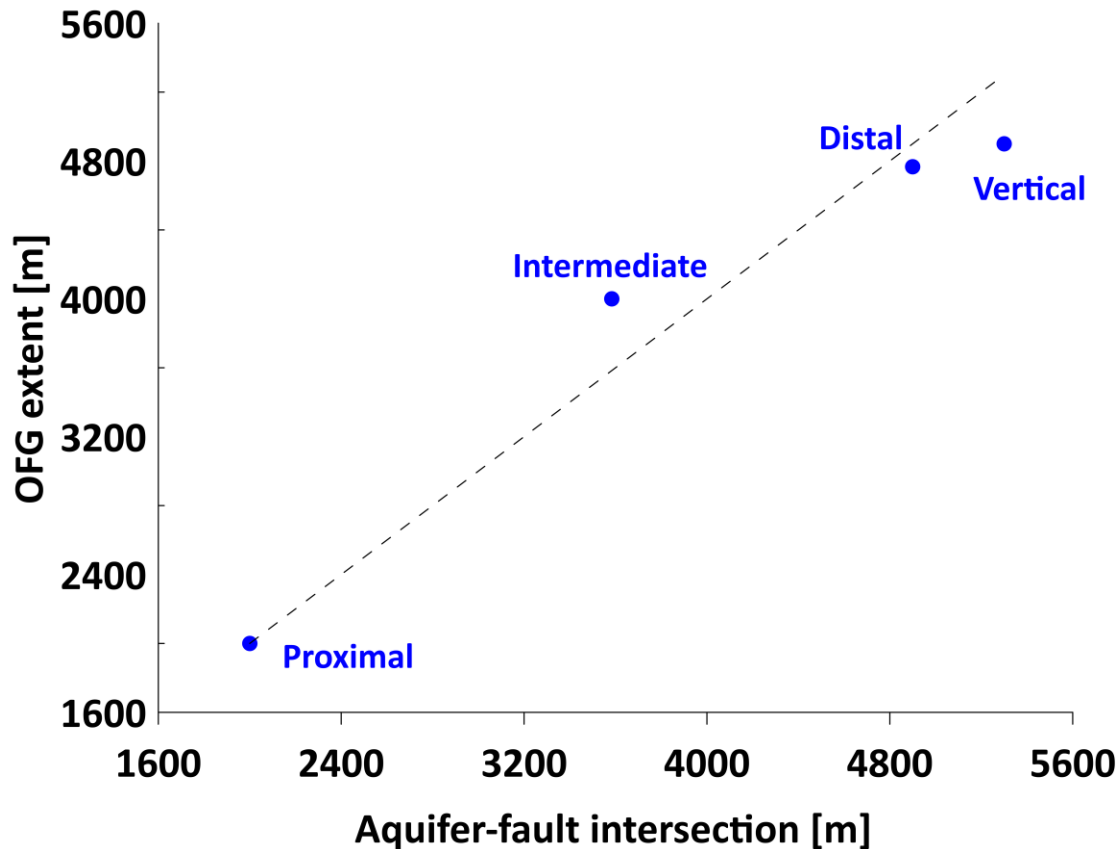
370



372 *Figure 6: (a) Initial and (b&c) final simulated salinities for two fault locations: (b) Distal (fault*  
373 *intersects the seafloor at a water of depth of 1000 mbsl) and (c) Proximal (fault intersects the*  
374 *seafloor at a water depth of 350 mbsl). Vertical black lines denote the intersection of the 50%*  
375 *salinity contour and the top of the aquifer (shaded). In both cases plotted here, the initial*  
376 *interface (a) is landward of the fault (i.e., fault starts saline). The final salinities (b&c) in the*  
377 *aquitard are masked to distinguish from the aquifer salinities. Note that the faults are marked*  
378 *here with a dashed line that extends beyond the seafloor for visibility purposes only. See Section*  
379 *3 above for detailed explanation of the fault implementation in the model.*

380  
381 In cases where the initial salinities dictate a fault-controlled OFG, the relationship between the  
382 location of the fault-aquifer intersection and the extent of OFG is evident across all simulated  
383 faults (Fig. 7). In Figure 7, points that are below the 1:1 line mean that the furthest offshore  
384 extent of freshened groundwater is less than the distance of the fault-aquifer intersection, and  
385 vice versa. Since the aquifer-fault intersection is the location where fresh, terrestrial groundwater  
386 potentially discharges from the aquifer up toward the sea, one might expect a 1:1 relationship,  
387 but that is not the case. As the fault location is further offshore, this relationship weakens and the  
388 seaward reach of OFG is less than predicted by the 1:1 line. In the case of a proximal vertical  
389 fault, the intersection with the aquifer is 500 m seaward of its location with a tilted fault, but the  
390 OFG reaches only ~150 m further offshore. This means that it is not only the aquifer-fault  
391 intersection that controls OFG, since the vertical fault cuts the aquifer further offshore but the  
392 impact on the offshore extent of OFG is minimal.

393  
394



395

396 *Figure 7: The extent of OFG as a function of the location of the aquifer-fault intersection. The*  
 397 *extent of OFG is defined as the maximum distance offshore of the 50% salinity contour in the*  
 398 *aquifer (Figures 4-6). Dashed line is the 1:1 line.*

399

## 400 5. Discussion and conclusions

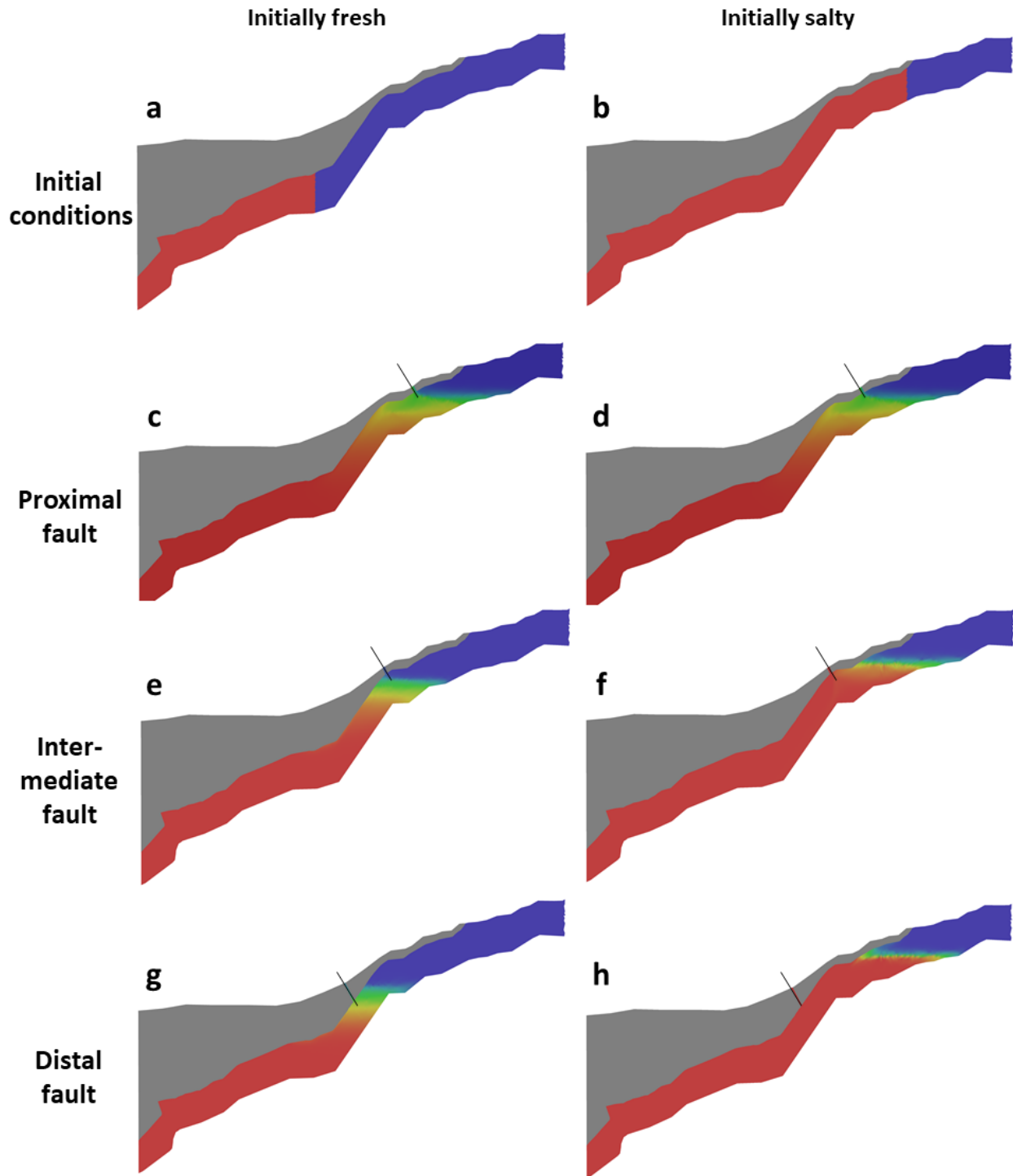
401

402 Previous studies of OFG considered only two modes of active or passive OFG (Fig. 1) (Cohen  
 403 et al., 2010; Haroon et al., 2021; Kooi & Groen, 2001; Post et al., 2013). Here, a novel  
 404 mechanism for OFG is found, which is an intermediate mode. The fault-controlled OFG  
 405 simulated here is continuous from the recharge area to the offshore, along a subsurface hydraulic  
 406 connection, but it depends on antecedent conditions (Fig. 8). As the main current challenge in  
 407 assessing the value of OFG reservoirs as a resource relies on understanding their underlying  
 408 hydrogeologic dynamics, this study presents a crucial step toward better understanding of the  
 409 ways in which OFG can be generated. In many studies, OFG is detected through observational  
 410 methods such as geophysics, hydrographic surveys, chemical sampling, or offshore drilling  
 411 (Attias et al., 2021; Hathaway et al., 1979; Micallef et al., 2020; Paldor et al., 2020a), but the  
 412 hydrogeological regimes that generate them are often not explored. The distinction between  
 413 active and passive OFG is important because active systems are likely renewable and hence  
 414 represent a more sustainable resource for extraction. However, a third type of system is  
 415 introduced here, which we call *conditional* active since there is a geologic connection, but active  
 416 flow depends on the hydrologic history. One example of a potential implication of this novel  
 417 *conditional* OFG is that extraction of offshore freshened groundwater from a system with

418 geologic connection may have a tipping point – while the steady state of the system could  
419 include onshore-offshore flow, pumping could pull saltwater and form the density-driven barrier  
420 that would inhibit active flow even if pumping is ceased. It is important to note that such a  
421 conditional OFG may form regardless of faults, if the geological structure is such that there is a  
422 U-shaped aquifer with an inlet onshore and an outlet offshore. In such cases, the initial  
423 conditions have the potential to dictate whether a density-driven barrier will form and inhibit  
424 fresh groundwater flow to the outlet. Further exploration is suggested here into these types of  
425 *conditional* OFG systems and their dominating factors.

426  
427 Assessments of modern OFG reservoirs that do not consider faults may erroneously estimate  
428 the extent of OFG, as fault locations and configuration may strongly control the offshore salinity  
429 distribution (Fig. 8). This is particularly important since faults are often neglected in large-scale  
430 hydrogeological studies (e.g., Paldor et al., 2019; Paldor et al., 2020b) since they are difficult to  
431 map and to model. However, the present work implies that ignoring faults may mean not only  
432 underestimating the extents of OFG, but a completely misinterpreting the onshore-offshore  
433 hydrogeologic regime. This can be seen in Figure 6, as the salinity transition zone that develops  
434 independent of a fault (Fig. 6b) is much narrower than the transition zone that develops in the  
435 vicinity of a fault (Fig. 6c). This means stronger density gradients and higher rates of buoyancy-  
436 driven flow even into the terrestrial domain of the aquifer. In other words, onshore wells that  
437 monitor the groundwater state may be impacted by offshore faults, regardless of the question of  
438 OFG extent.

439 The fault control on OFG is dependent on the initial salinity distribution (Fig. 8). This  
440 conditional relationship is important to consider in the context of modeling sea-level  
441 fluctuations, suggesting a hysteresis effect by which sea-level rise and sea-level drop may not  
442 have symmetrical effects on subsurface salinities when faults cut through confined subsea  
443 aquifers (fault starts fresh vs fault starts saline). In this work we did not model such processes  
444 explicitly, but the conclusions drawn here imply that this hysteresis effect should be considered  
445 when predicting modern salinities through simplifying assumptions on antecedent conditions.  
446 This effect stems from the buoyancy force – when the fault starts seaward of the interface, then  
447 the saline groundwater wedge acts as a density-driven flow barrier for the fresh groundwater  
448 recharging into the aquifer. Thus, the freshened groundwater never reaches the fault. Conversely,  
449 when the fault initially intersects the aquifer in a freshened area, direct flow of terrestrial  
450 groundwater is generated because the density-driven flow barrier is seaward of the fault, and this  
451 onshore-offshore flow keeps the transition zone seaward of the fault even in steady state. In the  
452 context of modeling OFG systems, which is a tool that is very widely used (Kooi & Groen, 2001;  
453 Paldor et al., 2020b; Person et al., 2003), simplifying assumptions on initial salinities are often  
454 adopted to achieve numerical stability. This work suggests that initial conditions adopted in  
455 modeling OFG are a crucial factor and strongly influences the final result.



456

457 *Figure 8: A comparison of the final salinity distributions with the three fault scenarios (proximal, intermediate, and distal),*  
 458 *with initial conditions of faults penetrating freshwater (left, panels a,c,e,g) and initially penetrating saltwater (right, panels*  
 459 *b,d,f,h). Thin black lines mark the fault location. Salinities in the aquitard are greyed out to facilitate comparisons between*  
 460 *aquifer salinities only.*

461

462 It should be noted that there are two factors that likely impact the fault-dominated salinity  
463 distribution. The first factor is the offshore distance of the fault-aquifer intersection, which  
464 dictates the overall land-to-sea gradient. For a given recharge rate on land and a given (upward)  
465 percolation rate across the confining unit, a more distal fault experiences a weaker “push” of  
466 freshwater toward it from land (when initial conditions dictate that freshwater ever reaches it).  
467 The second factor is the head gradient along the fault. Since the freshwater-equivalent head  
468 increases with seafloor depth (due to greater thicknesses of the denser seawater column), faults  
469 that cut the seafloor at greater water depths have higher heads at their top. Therefore, it is not  
470 only the fault-seafloor intersection that is important to consider, but also the geometry of the  
471 fault and its intersection with the aquifer. This likely introduces great challenges since offshore  
472 geophysical data quality strongly reduces with depth below the surface, meaning that this crucial  
473 factor may be very hard to predict.

474  
475 The findings of this study should be considered in future explorations of OFG, which rely  
476 heavily on understanding the hydrogeological mechanisms for onshore-offshore transport of  
477 freshened groundwater. Furthermore, modeling OFG systems should take in consideration the  
478 critical dependency of the simulated dynamics on the adopted approach (initial conditions, fault  
479 representation, etc.). Better understanding the dynamics of flow and transport in OFG systems  
480 and better modeling approaches have important global implications for water resources  
481 management, seafloor geomorphology, and marine biogeochemistry.

#### 482 **Acknowledgments**

483 This work was partly funded by the National Science Foundation, Coastal Critical Zone  
484 Network, grant number CZN - NSF EAR2012484.

485 This publication is also based upon work from COST Action OFF-Source, CA21112, supported  
486 by COST (European Cooperation in Science and Technology).

#### 487 **References**

- 488  
489  
490 Anderson, E. M. (1905). The dynamics of faulting. *Transactions of the Edinburgh Geological*  
491 *Society*, 8(3), 387–402. <https://doi.org/10.1144/transed.8.3.387>
- 492 Attias, E., Constable, S., Sherman, D., Ismail, K., Shuler, C., & Dulai, H. (2021). Marine  
493 Electromagnetic Imaging and Volumetric Estimation of Freshwater Plumes Offshore  
494 Hawai'i. *Geophysical Research Letters*, 48(7), e2020GL091249.  
495 <https://doi.org/10.1029/2020GL091249>
- 496 Attias, E., Thomas, D., Sherman, D., Ismail, K., & Constable, S. (2020). Marine electrical  
497 imaging reveals novel freshwater transport mechanism in Hawai'i. *Science Advances*, 6(48).  
498 <https://doi.org/10.1126/sciadv.abd4866>
- 499 Avisar, D., Rosenthal, E., Shulman, H., Zilberbrand, M., Flexer, A., Kronfeld, J., ... & Fleischer,  
500 L. (2004). The Pliocene Yafo Formation in Israel: hydrogeologically inert or  
501 active?. *Hydrogeology Journal*, 12, 291-304.
- 502 Bakalowicz, M., El Hakim, M., & El-Hajj, A. (2008). Karst groundwater resources in the  
503 countries of eastern Mediterranean: The example of Lebanon. *Environmental Geology*,  
504 54(3), 597–604. <https://doi.org/10.1007/s00254-007-0854-z>
- 505 Bein, A., and G. Gvirtzman. (1977). a mesozoic fossil edge of the arabian plate along the levant  
506 coastline and its bearing on the evolution of the eastern mediterranean.
- 507 Bense, V. F., Gleeson, T., Loveless, S. E., Bour, O., & Scibek, J. (2013). Fault zone

508 hydrogeology. *Earth-Science Reviews*, 127, 171–192.  
509 <https://doi.org/10.1016/j.earscirev.2013.09.008>

510 Bratton, J. F. (2010). The Three Scales of Submarine Groundwater Flow and Discharge across  
511 Passive Continental Margins. *The Journal of Geology*, 118(5), 565–575.  
512 <https://doi.org/10.1086/655114>

513 Carton, H., Singh, S. C., Tapponnier, P., Elias, A., Briais, A., Sursock, A., ... & Barrier, L.  
514 (2009). Seismic evidence for Neogene and active shortening offshore of Lebanon (Shalimar  
515 cruise). *Journal of Geophysical Research: Solid Earth*, 114(B7).

516 Cohen, D., Person, M., Wang, P., Gable, C. W., Hutchinson, D., Marksamer, A., ... Lane, J. W.  
517 (2010). Origin and extent of fresh paleowaters on the Atlantic continental shelf, USA.  
518 *Ground Water*. <https://doi.org/10.1111/j.1745-6584.2009.00627.x>

519 Dafny, E., Burg, A., & Gvirtzman, H. (2010). Effects of Karst and geological structure on  
520 groundwater flow: The case of Yarqon-Taninim Aquifer, Israel. *Journal of*  
521 *hydrology*, 389(3-4), 260-275. Dugan, B., & Flemings, P. B. (2002). Fluid flow and stability  
522 of the US continental slope offshore New Jersey from the Pleistocene to the present.  
523 *Geofluids*, 2(2), 137–146. <https://doi.org/10.1046/j.1468-8123.2002.00032.x>

524 Elasar, M., Kerem, D., Angel, D., Steindler, L., Herut, B., Barnea, O., & Almogi, A. (2013).  
525 Achziv Submarine Canyon: an Oasis in the Warming Oligotrophic Levantine Basin? In  
526 *Rapp. Comm. int. Mer Médit.* (Vol. 40, p. 2013). Retrieved from  
527 [http://www.ciesm.org/online/archives/abstracts/pdf/40/PG\\_0718.pdf](http://www.ciesm.org/online/archives/abstracts/pdf/40/PG_0718.pdf)

528 Fleury, P., Bakalowicz, M., & de Marsily, G. (2007). Submarine springs and coastal karst  
529 aquifers: A review. *Journal of Hydrology*, 339(1–2), 79–92.  
530 <https://doi.org/10.1016/j.jhydrol.2007.03.009>

531 Freeze, R. A., & Cherry, J. A. (1979). *Groundwater*. Prentice-Hall.

532 Gardosh, M. A., & Druckman, Y. (2006). Seismic stratigraphy, structure and tectonic evolution  
533 of the Levantine Basin, offshore Israel. Geological Society, London, Special Publications,  
534 260(1), 201-227.

535 Gelhar, L. W., Welty, C., & Rehfeldt, K. R. (1992). A Critical Review of Data on Field-Scale  
536 Dispersin in Aquifers. *Water Resources Research*, 28(7), 1955–1974.  
537 <https://doi.org/10.1029/92WR00607>

538 Gustafson, C., Key, K., & Evans, R. L. (2019). Aquifer systems extending far offshore on the  
539 U.S. Atlantic margin. *Scientific Reports*, 9(1), 8709. <https://doi.org/10.1038/s41598-019-44611-7>

540

541 Haroon, A., Micallef, A., Jegen, M., Schwalenberg, K., Karstens, J., Berndt, C., ... Chidichimo,  
542 F. (2021). Electrical Resistivity Anomalies Offshore a Carbonate Coastline: Evidence for  
543 Freshened Groundwater? *Geophysical Research Letters*, 48(14), e2020GL091909.  
544 <https://doi.org/10.1029/2020GL091909>

545 Hathaway, J. C., Poag, C. W., Valentine, P. C., Miller, R. E., Schultz, D. M., Manheim, F. T., ...  
546 Sangrey, D. A. (1979). U.S. geological survey core drilling on the Atlantic shelf. *Science*.  
547 <https://doi.org/10.1126/science.206.4418.515>

548 Hawie, N., Gorini, C., Deschamps, R., Nader, F. H., Montadert, L., Granjeon, D., & Baudin, F.  
549 (2013). Tectono-stratigraphic evolution of the northern Levant Basin (offshore  
550 Lebanon). *Marine and petroleum geology*, 48, 392-410.

551 Iverson, R. M., & Reid, M. E. (1992). Gravity driven groundwater flow and slope failure  
552 potential: 1. Elastic Effective Stress Model. *Water Resources Research*, 28(3), 925–938.  
553 <https://doi.org/10.1029/91WR02694>

- 554 Kafri, U., & Fleischer, L. (2003). Structural mapping as a tool for hydrogeological modeling,  
555 judea group aquifers, western galilee, israel. *Geol. Surv. Isr. Cur. Res*, 13, 52–58.
- 556 Kafri, U., & Kessler, A. (2001). *Hydrogeological Plan for the Development, Production and*  
557 *Exploitation of the Kabri Basin*. Jerusalem, Israel.
- 558 Kafri, Uri. (1972). Lithostratigraphy and environment of deposition, Judea Group, western and  
559 central Galilee, Israel. Jerusalem, Israel: Isr. Geol. Surv. Bull.
- 560 Kelner, M., Migeon, S., Tric, E., Couboulex, F., Dano, A., Lebourg, T., & Taboada, A. (2016).  
561 Frequency and triggering of small-scale submarine landslides on decadal timescales:  
562 analysis of 4D bathymetric data from the continental slope offshore Nice (France). *Marine*  
563 *Geology*, 379, 281-297.
- 564 Kessler, A., & Kafri, U. (2008). Application of a cell model for operational management of the  
565 Na’aman groundwater basin, Israel. *Israel Journal of Earth Sciences*, 56(1), 29–46.  
566 <https://doi.org/10.1560/IJES.56.1.29>
- 567 Kooi, H., & Groen, J. (2001). Offshore continuation of coastal groundwater systems; predictions  
568 using sharp-interface approximations and variable-density flow modelling. *Journal of*  
569 *Hydrology*, 246, 19–35. Retrieved from [http://ac.els-cdn.com/S0022169401003547/1-s2.0-S0022169401003547-main.pdf?\\_tid=b03b4e90-e27c-11e3-9d4f-00000aab0f01&acdnat=1400851271\\_162dbbca606b23a4c84fe231c2b1bb62%5Cnhttp://www.sciencedirect.com/science/article/pii/S0022169401003547](http://ac.els-cdn.com/S0022169401003547/1-s2.0-S0022169401003547-main.pdf?_tid=b03b4e90-e27c-11e3-9d4f-00000aab0f01&acdnat=1400851271_162dbbca606b23a4c84fe231c2b1bb62%5Cnhttp://www.sciencedirect.com/science/article/pii/S0022169401003547)
- 571 <http://www.sciencedirect.com/science/article/pii/S0022169401003547>
- 572 [www.sciencedirect.com/science/article/pii/S0022169401003547](http://www.sciencedirect.com/science/article/pii/S0022169401003547)
- 573 Li, L., Barry, D. A., Stagnitti, F., & Parlange, J. Y. (1999). Submarine groundwater discharge  
574 and associated chemical input to a coastal sea. *Water Resources Research*, 35(11), 3253–  
575 3259. <https://doi.org/10.1029/1999WR900189>
- 576 Luijendijk, E., Gleeson, T., & Moosdorf, N. (2020). Fresh groundwater discharge insignificant  
577 for the world’s oceans but important for coastal ecosystems. *Nature Communications*,  
578 11(1). <https://doi.org/10.1038/s41467-020-15064-8>
- 579 Micallef, A., Person, M., Gupta, S., Saadatkhah, N., Camille, A., & Gratacós, Ò. (2023). Can  
580 Offshore Meteoric Groundwater Generate Mechanical Instabilities in Passive Continental  
581 Margins? *Journal of Geophysical Research: Earth Surface*, 128(3), e2022JF006954.  
582 <https://doi.org/10.1029/2022jf006954>
- 583 Micallef, A., Person, M., Haroon, A., Weymer, B. A., Jegen, M., Schwalenberg, K., Faghih, Z.,  
584 Duan, S., Cohen, D., Mountjoy, J.J., Woelz, S., Gable, C.W., Avers, T., Kumar Tiwari, A.  
585 (2020). 3D characterisation and quantification of an offshore freshened groundwater system  
586 in the Canterbury Bight. *Nature Communications*. [https://doi.org/10.1038/s41467-020-](https://doi.org/10.1038/s41467-020-14770-7)  
587 [14770-7](https://doi.org/10.1038/s41467-020-14770-7)
- 588 Moore, W. S. (2010). The effect of submarine groundwater discharge on the ocean. *Annual*  
589 *Review of Marine Science*, 2, 59–88. [https://doi.org/10.1146/annurev-marine-120308-](https://doi.org/10.1146/annurev-marine-120308-081019)  
590 [081019](https://doi.org/10.1146/annurev-marine-120308-081019)
- 591 Oehler, T., Mogollón, J. M., Moosdorf, N., Winkler, A., Kopf, A., & Pichler, T. (2017).  
592 Submarine groundwater discharge within a landslide scar at the French Mediterranean  
593 coast. *Estuarine, Coastal and Shelf Science*, 198, 128–137.  
594 <https://doi.org/10.1016/j.ecss.2017.09.006>
- 595 Oehler, T., Mogollón, J. M., Moosdorf, N., Winkler, A., Kopf, A., & Pichler, T. (2017).  
596 Submarine groundwater discharge within a landslide scar at the French Mediterranean  
597 coast. *Estuarine, Coastal and Shelf Science*, 198, 128-137.
- 598 Orange, D. L., Anderson, R. S., & Breen, N. A. (1994). Regular Canyon Spacing in the  
599 Submarine Environment: The Link Between Hydrology and Geomorphology. *Geological*

600 *Society of America Bulletin*, 4(2), 35–39.

601 Orange, D. L., Yun, J., Maher, N., Barry, J., & Greene, G. (2002). Tracking California seafloor  
602 seeps with bathymetry, backscatter and ROVs. *Continental Shelf Research*, 22(16), 2273–  
603 2290. [https://doi.org/10.1016/S0278-4343\(02\)00054-7](https://doi.org/10.1016/S0278-4343(02)00054-7)

604 Paldor, A., Aharonov, E., & Katz, O. (2020b). Thermo-haline circulations in subsea confined  
605 aquifers produce saline, steady-state deep submarine groundwater discharge. *Journal of*  
606 *Hydrology*, 580. <https://doi.org/10.1016/j.jhydrol.2019.124276>

607 Paldor, A., Katz, O., Aharonov, E., Weinstein, Y., Roditi-Elasar, M., Lazar, A., & Lazar, B.  
608 (2020a). Deep Submarine Groundwater Discharge—Evidence From Achziv Submarine  
609 Canyon at the Exposure of the Judea Group Confined Aquifer, Eastern Mediterranean.  
610 *Journal of Geophysical Research: Oceans*, 125(1). <https://doi.org/10.1029/2019JC015435>

611 Paldor, A., Shalev, E., Katz, O., & Aharonov, E. (2019). Dynamics of saltwater intrusion and  
612 submarine groundwater discharge in confined coastal aquifers: a case study in northern  
613 Israel. *Hydrogeology Journal*, 27(5), 1611–1625. <https://doi.org/10.1007/s10040-019-01958-5>

614

615 Person, M., Dugan, B., Swenson, J. B., Urbano, L., Stott, C., Taylor, J., & Willett, M. (2003).  
616 Pleistocene hydrogeology of the Atlantic continental shelf, New England. *Bulletin of the*  
617 *Geological Society of America*, 115(11), 1324–1343. <https://doi.org/10.1130/B25285.1>

618 Person, M., Wilson, J. L., Morrow, N., & Post, V. E. A. (2017). Continental-shelf freshwater  
619 water resources and improved oil recovery by low-salinity waterflooding. *AAPG Bulletin*.  
620 <https://doi.org/10.1306/05241615143>

621 Post, V. E. A., Groen, J., Kooi, H., Person, M., Ge, S., & Edmunds, W. M. (2013). Offshore  
622 fresh groundwater reserves as a global phenomenon. *Nature*, 504(7478), 71–78.  
623 <https://doi.org/10.1038/nature12858>

624 Schorghofer, N., Jensen, B., Kudrolli, A., & Rothman, D. H. (2004). Spontaneous channelization  
625 in permeable ground: theory, experiment, and observation. *Journal of Fluid Mechanics*,  
626 503(503), 357–374. <https://doi.org/10.1017/S0022112004007931>

627 Sebben, M. L., Werner, A. D., & Graf, T. (2015). Seawater intrusion in fractured coastal  
628 aquifers: A preliminary numerical investigation using a fractured Henry problem. *Advances*  
629 *in Water Resources*, 85, 93–108. <https://doi.org/10.1016/j.advwatres.2015.09.013>

630 Shaban, A., Khawlie, M., Abdallah, C., & Faour, G. (2005). Geologic controls of submarine  
631 groundwater discharge: Application of remote sensing to north Lebanon. *Environmental*  
632 *Geology*, 47(4), 512–522. <https://doi.org/10.1007/s00254-004-1172-3>

633 Stanic, S., LeRoux, N. K., Paldor, A., Mohammed, A. A., Michael, H. A., & Kurylyk, B. L.  
634 (2024). Saltwater Intrusion Into a Confined Island Aquifer Driven by Erosion, Changing  
635 Recharge, Sea-Level Rise, and Coastal Flooding. *Water Resources Research*, 60(1),  
636 e2023WR036394.

637 Stegmann, S., Sultan, N., Kopf, a., Apprioual, R., & Pelleau, P. (2011). Hydrogeology and its  
638 effect on slope stability along the coastal aquifer of Nice, France. *Marine Geology*, 280(1–  
639 4), 168–181. <https://doi.org/10.1016/j.margeo.2010.12.009>

640 Sultan, N., Garziglia, S., Bompais, X., Woerther, P., Witt, C., Kopf, A., & Migeon, S. (2020).  
641 Transient groundwater flow through a coastal confined aquifer and its impact on nearshore  
642 submarine slope instability. *Journal of Geophysical Research: Earth Surface*, 125(9),  
643 e2020JF005654.

644 Vengosh, A., & Ben-Zvi, A. (1994). Formation of a salt plume in the Coastal Plain aquifer of  
645 Israel: the Be'er Toviyya region. *Journal of Hydrology*, 160(1-4), 21-52.

- 646 Xu, Z., Hu, B. X., & Ye, M. (2018). Numerical modeling and sensitivity analysis of seawater  
647 intrusion in a dual-permeability coastal karst aquifer with conduit networks. *Hydrology and*  
648 *Earth System Sciences*, 22(1), 221–239. <https://doi.org/10.5194/hess-22-221-2018>
- 649 Yechieli, Y., Kafri, U., & Sivan, O. (2009). The inter-relationship between coastal sub-aquifers  
650 and the Mediterranean Sea, deduced from radioactive isotopes analysis. *Hydrogeology*  
651 *Journal*, 17(2), 265–274. <https://doi.org/10.1007/s10040-008-0329-7>
- 652 Yu, X., & Michael, H. A. (2019). Offshore Pumping Impacts Onshore Groundwater Resources  
653 and Land Subsidence. *Geophysical Research Letters*.  
654 <https://doi.org/10.1029/2019GL081910>